



Since January 2020 Elsevier has created a COVID-19 resource centre with free information in English and Mandarin on the novel coronavirus COVID-19. The COVID-19 resource centre is hosted on Elsevier Connect, the company's public news and information website.

Elsevier hereby grants permission to make all its COVID-19-related research that is available on the COVID-19 resource centre - including this research content - immediately available in PubMed Central and other publicly funded repositories, such as the WHO COVID database with rights for unrestricted research re-use and analyses in any form or by any means with acknowledgement of the original source. These permissions are granted for free by Elsevier for as long as the COVID-19 resource centre remains active.



Dual targeting powder formulation of antiviral agent for customizable nasal and lung deposition profile through single intranasal administration

Han Cong Seow^a, Qiuying Liao^a, Andy T.Y. Lau^a, Susan W.S. Leung^a, Shuofeng Yuan^{b,c}, Jenny K.W. Lam^{a,d,*}

^a Department of Pharmacology and Pharmacy, LKS Faculty of Medicine, The University of Hong Kong, Pokfulam, Hong Kong SAR

^b State Key Laboratory of Emerging Infectious Diseases, Caro Yu Centre for Infection, Department of Microbiology, LKS Faculty of Medicine, The University of Hong Kong, Pokfulam, Hong Kong SAR

^c Centre for Virology, Vaccinology and Therapeutics, Hong Kong Science Park, New Territories, Hong Kong SAR

^d Advanced Biomedical Instrumentation Centre, Hong Kong Science Park, New Territories, Hong Kong SAR

ARTICLE INFO

Keywords:

Antiviral agent
COVID-19
Dry powder aerosol
Intranasal delivery
Pulmonary delivery
Spray drying
Spray freeze drying

ABSTRACT

Unpredictable outbreaks due to respiratory viral infections emphasize the need for new drug delivery strategies to the entire respiratory tract. As viral attack is not limited to a specific anatomic region, antiviral therapy that targets both the upper and lower respiratory tract would be most effective. This study aimed to formulate tamibarotene, a retinoid derivative previously reported to display broad-spectrum antiviral activity against influenza and severe acute respiratory syndrome coronavirus-2 (SARS-CoV-2), as a novel dual particle size powder formulation that targets both the nasal cavity and the lung by a single route of intranasal administration. Spray freeze drying (SFD) and spray drying (SD) techniques were employed to prepare tamibarotene powder formulations, and cyclodextrin was used as the sole excipient to enhance drug solubility. With the employment of appropriate atomizing nozzles, particles of size above 10 μm and below 5 μm could be produced for nasal and lung deposition, respectively. The aerosol performance of the powder was evaluated using Next Generation Impactor (NGI) coupled with a glass expansion chamber and the powder was dispersed with a nasal powder device. By blending powder of two different particle sizes, a single powder formulation with dual aerosol deposition characteristic in both the nasal and pulmonary regions was produced. The aerosol deposition fractions in the nasal cavity and pulmonary region could be modulated by varying the powder mixing ratio. All dry powder formulations exhibited spherical structures, amorphous characteristics and improved dissolution profile as compared to the unformulated tamibarotene. Overall, a novel dual targeting powder formulation of tamibarotene exhibiting customizable aerosol deposition profile was developed. This exceptional formulation strategy can be adopted to deliver other antimicrobial agents to the upper and lower airways for the prevention and treatment of human respiratory infections.

1. Introduction

Airborne viruses are serious global threats that cause a multitude of respiratory diseases. Influenza, rhinovirus, adenovirus, and coronavirus are common causes of viral respiratory infections that are highly contagious and potentially deadly. The new severe acute respiratory

syndrome coronavirus-2 (SARS-CoV-2) most recently caused the Coronavirus Disease 2019 (COVID-19) pandemic due to its rapid spread and devastating impact (Platto et al., 2020). The unprecedented spread of SARS-CoV-2 can be attributed to high viral shedding in the upper respiratory tract of asymptomatic or pre-symptomatic individuals at an early stage of infection (Wu et al., 2021). The transmission of SARS-CoV-

Abbreviations: ACE2, Angiotensin-converting enzyme 2; COVID19, Coronavirus disease 2019; DSC, Differential scanning calorimetry; EF, Emitted fraction; FPF, Fine particle fraction; HPBCD, 2-hydroxypropyl- β -cyclodextrin; MERS-CoV, Middle East respiratory syndrome coronavirus; NF, Nasal fraction; NGI, Next Generation Impactor; RF, Residual fraction; SARS-CoV-2, Severe acute respiratory syndrome coronavirus-2; SD, Spray drying; SEM, Scanning electron microscopy; SFD, Spray freeze drying; SREBP, Sterol regulatory element binding protein; TBA, Tert-Butyl alcohol; TF, Throat fraction; TGA, Thermogravimetric analysis; TFN, Two-fluid nozzle; USN, Ultrasonic nozzle.

* Corresponding author at: Department of Pharmacology and Pharmacy, LKS Faculty of Medicine, The University of Hong Kong, Pokfulam, Hong Kong SAR.

E-mail address: jkwlam@hku.hk (J.K.W. Lam).

<https://doi.org/10.1016/j.ijpharm.2022.121704>

Received 23 January 2022; Received in revised form 4 March 2022; Accepted 24 March 2022

Available online 28 March 2022

0378-5173/© 2022 The Author(s). Published by Elsevier B.V. This is an open access article under the CC BY-NC-ND license (<http://creativecommons.org/licenses/by-nc-nd/4.0/>).

2 through airborne respiratory droplets and aerosols (Liu et al., 2020) highlights the importance of developing new methods that target the entire respiratory tract for preventing transmission, contraction, and rapid treatment of COVID-19.

Spike proteins on the SARS-CoV-2 viral membrane facilitate viral entry into the host cell (Zhao et al., 2020) and have strong affinity to angiotensin-converting enzyme 2 (ACE2) receptors that are highly expressed on respiratory cells (Shang et al., 2020). As ACE2 receptors are found to be expressed highest in the nasal cavity with decreasing expression from the upper to lower respiratory tract, the infectivity of SARS-CoV-2 also gradually decreases from the proximal to distal respiratory tract (Hou et al., 2020). Thus, the nasal epithelium is potentially the origin of infection and acts as a viral reservoir that subsequently spreads the virus across the respiratory mucosa by aspiration-mediated virus seeding (Hou et al., 2020). Aerosolized droplets containing SARS-CoV-2 virus may also directly enter the deep lung region causing severe infection, cytokine dysregulation and acute respiratory distress syndrome (Salian et al., 2021). Studies showed that there is more persistent viral shedding in the lower respiratory tract in COVID-19 patients (Wang et al., 2020). Hence, targeting both the upper and lower respiratory tract is critical for the treatment of COVID-19 infections by maximising drug concentration at the sites of maximal viral load (Sungnak et al., 2020). In addition, nasal administration of antiviral agents can have the added benefit of reducing the spread of SARS-CoV-2 to the brain through the olfactory mucosa in the nasal cavity (Baig, 2021; Meinhardt et al., 2021). Coinfection with other viruses such as influenza also further complicates the disease, with interferon-driven upregulation of ACE2 in nasal epithelia and lung tissue increasing the susceptibility of the respiratory tract to SARS-CoV-2 infection (Ziegler et al., 2020). Considering the unpredictability of viral pandemics, early administration of a broad-spectrum antiviral agent that targets both the upper and lower respiratory tract would be an effective strategy for the treatment and control of viral infections and co-infections.

In attempt to control the pandemic, nasal vaccines are being investigated to curb viral spread by inducing immunity in the airways (Zhao et al., 2020). New therapeutic agents such as fusion inhibitors (de Vries et al., 2021), acidic electrolyzed water (Takeda et al., 2020) and nitric oxide (Winchester et al., 2021) have been studied to directly target the virus present in the nasal cavity. According to our previous study, an inhalable dry powder formulation of tamibarotene was shown to have broad spectrum antiviral activity against SARS-CoV-2, Middle East respiratory syndrome coronavirus (MERS-CoV) and Influenza A virus (Liao et al., 2021). Tamibarotene is a retinoid derivative that triggers lipid metabolic reprogramming by interacting with the sterol regulatory element binding protein (SREBP) in host cells (Yuan et al., 2019). The suppression of lipogenesis results in reduced double-membrane vesicles and viral protein palmitoylation, thereby interfering with viral entry and multiplication (Yuan et al., 2020). Marketed as an oral tablet, tamibarotene is chemically stable and has a known safety profile in humans due to its clinical use for acute promyelocytic leukaemia (Miwako and Kagechika, 2007). Pulmonary delivery of tamibarotene reduces unintended systemic exposure and increases drug concentration in the airway which is the primary site of infection, thereby increasing its efficacy as a broad-spectrum antiviral agent.

Spray freeze drying (SFD) and spray drying (SD) are particle engineering techniques for producing dry powder formulations. The former is a two-stage process of spraying the feed solution into liquid nitrogen for flash freezing of atomized droplets, followed by sublimation of the frozen solvent at low temperature and pressure. The latter is a continuous and scalable process that atomizes liquid feed into hot air for instantaneous evaporation of the solvent. Both techniques can be optimised to produce particles with desirable particle size, morphology, and aerosol properties for efficient targeted drug delivery (Emami et al., 2018; Leung et al., 2016; Liao et al., 2019; Liao et al., 2020). In this study, we aimed to develop a novel dual targeting powder formulation of tamibarotene that targets both the upper and lower respiratory tract

simultaneously by a single route of intranasal administration. Although the administration of powder aerosol to the lung through a nasal high-flow system has been previously investigated (Longest et al., 2015; Okuda et al., 2017), delivery of dry powder to the upper and lower airways with a portable handheld nasal powder device for insufflation has not been reported. 2-hydroxypropyl- β -cyclodextrin (HPBCD) is a cyclic oligosaccharide with good safety profile, including by nasal and pulmonary administration (Jansook et al., 2018; Kim et al., 2020). Here, HPBCD was used as excipient to form water soluble inclusion complexes with the insoluble tamibarotene, which was reformulated as powder aerosols using SFD or SD technique with specific particle size ranges. The ultrasonic nozzle was employed to produce large particles aimed for nasal deposition whereas the two-fluid nozzle was employed to generate small particles aimed for lung deposition. By blending two powder formulations of different particle size ranges, a dual targeting formulation of tamibarotene capable of depositing at both the nasal and the lung regions was developed. Different mixing ratios of the dual particle size formulation were tested to determine how the aerosol performance of the powder blend can be controlled to achieve desirable aerosol deposition profile at the target sites.

2. Materials and methods

2.1. Materials

Tamibarotene was purchased from Dalian Meilun Biotechnology Co., Ltd (Dalian, China). HPBCD was purchased from Sigma-Aldrich (Saint Louis, USA). *Tert*-Butyl alcohol (TBA) was obtained from Meryer Chemical Technology (Shanghai, China). Ethanol was obtained from VWR BDH Chemicals (VWR International S.A.S., Fontenay-sous-Bois, France). Methanol and acetonitrile (HPLC grade) were purchased from Anaqua Chemicals Supply (Cleveland, USA). Glacial acetic acid was purchased from Fisher Scientific (Loughborough, UK). All solvents and reagents were of analytical grade unless otherwise specified.

2.2. Methods

2.2.1. Preparation of dry powder formulation by spray freeze drying (SFD)

Spray freeze drying (SFD) was carried out in a two-stage operation – spray freezing followed by freeze drying. The feed solution was prepared by dissolving tamibarotene and HPBCD at 30:70 ratio (w/w) in 55% TBA (v/v) to a final solute concentration of 4% (w/v) (Table 1). To prevent freezing of TBA (which has a freezing point of 25.4 °C), the solution was maintained at 37 °C before being loaded into a pre-warmed 10 mL syringe (TERUMO®, Philippines) that was connected to a syringe pump (LEGATO® 210 Syringe Pump, KD Scientific, MA, USA). The liquid feed rate was controlled at 1.5 mL/min. Half of the feed solution was atomized using a two-fluid nozzle (TFN; Büchi with an internal diameter of 0.7 mm, Switzerland) operated at a nitrogen gas flow rate of 601 L/h. The other half of the feed solution was atomized using an ultrasonic nozzle (USN; 130K50ST, Sonaer®, Farmingdale, NY, USA) operated at 130 kHz powered by a digital ultrasonic generator (Sonaer®, NY, USA). The sprayed droplets were instantly frozen in stainless-steel collectors containing liquid nitrogen and were then transferred into a pre-cooled freeze dryer (FreeZone® 6 Litre Benchtop Freeze Dry System with Stoppering Tray Dryer, Labconco Corporation, Missouri, USA). The freeze dryer was operated at a vacuum pressure below 0.14 mBar and programmed to maintain a primary drying temperature of –25 °C for 40 h, followed by gradually increasing to a secondary drying temperature of 20 °C in 4 h, and finally stabilized at room temperature for at least 20 h. The SFD powders produced by the two different nozzles were collected separately. The production yield was calculated as the percentage of total mass of powder collected to the initial solute mass in the feed solution. The powder was stored in a desiccator at room temperature before analysis.

Table 1

Formulations of tamibarotene dry powder produced by spray drying (SD) and spray freeze drying (SFD). *w/w ratio was used in the mixed formulations.

	Single formulations			
	SFD-USN	SFD-TFN	SD-USN	SD-TFN
Drying method	Spray drying		Spray freeze drying	
Nozzle	Ultrasonic (Sonaer®)		Ultrasonic (Büchi)	
Composition	Tamibarotene: HPBCD at 30:70 ratio (w/w)			
Solvent	55% v/v TBA		70% v/v ethanol	
Solute conc. (w/v)	4%	4%	2%	2%
Feed volume (mL)	5	5	25	25
Feed rate (mL/min)	1.5	1.5	2.4	1.2
Mixed formulations*	SFD-MIX-0.25	3	:	1
	SFD-MIX-1	1	:	1
	SFD-MIX-2	1	:	2
	SFD-MIX-3	1	:	3
	SFD-MIX-7	1	:	7
	SD-MIX-0.25			3
	SD-MIX-1			1
	SD-MIX-2			1
	SD-MIX-3			1
	SD-MIX-7			1

2.2.2. Preparation of dry powder formulation by spray drying (SD)

Spray drying was performed using a laboratory scale spray dryer with a high-performance cyclone in suction mode and closed loop configuration (Mini Spray Dryer B-290, Dehumidifier B-296 and Inert Loop B-295; Büchi Labortechnik, Flawil, Switzerland), with an inlet temperature of 150 °C and aspiration rate at 100% (approximately 35 m³/h). The feed solution for spray drying was prepared by dissolving tamibarotene and HPBCD at 30:70 ratio (w/w) in 70% ethanol (v/v) to a final solute concentration of 2% w/v (Table 1). Half of the feed solution was sprayed at a liquid feed rate of 1.2 mL/min with a two-fluid nozzle (TFN; Büchi with an internal diameter of 0.7 mm, Switzerland) controlled at a nitrogen gas flow rate of 601 L/h. The other half of the feed solution was sprayed at a liquid feed rate of 2.4 mL/min with an ultrasonic nozzle (USN; Büchi for particle size 10 to 60 µm, Switzerland) operated at 0.9 W. The SD powders produced by the two different nozzles were collected separately. The production yield was calculated as the percentage of total mass of powder collected to the initial solute mass in the feed solution. The powder was stored in a desiccator at room temperature before analysis.

2.2.3. Powder blending to produce dual targeting formulation

Dry powder formulations prepared with the same drying method but different atomization nozzle were mixed at different mass ratios using a Turbula® shaker-mixer type T2F (Willy A. Bachofen AG Maschinenfabrik, Basel, Switzerland) (Table 1). A total of 40 mg of powder was placed into a 50 mL glass vial and subjected to a constant rotational speed of 49 rpm. The mixing was carried out at room temperature and the samples were subjected to translational and rotational mixing for 10 min.

2.2.4. Morphology study using scanning electron microscopy (SEM)

The morphology of tamibarotene powder formulations was observed under the field emission SEM (Hitachi S-4800 N, Tokyo, Japan) at 5.0 kV. The powders were sprinkled onto carbon double-sided tape and mounted onto SEM stubs. Excess layers of powder were removed by tapping the stubs and blowing with clean compressed air. To avoid charging interferences during imaging, the stubs with samples were sputter-coated with approximately 13 nm of gold-palladium alloy in 90 s using a sputter coater (Q150T PLUS Turbomolecular Pumped Coater, Quorum, UK).

2.2.5. Drug quantification using high performance liquid chromatography (HPLC)

The amount of tamibarotene in each formulation was quantified using HPLC with photodiode array detector (Agilent 1260 Infinity; Santa

Clara, USA). The dry powders were weighed and dissolved in methanol to a final volume of 25 mL. The dissolved samples were filtered through a 0.45-µm nylon membrane filter and quantified using an established HPLC method (Liao et al., 2021). Briefly, a 25 µL sample was injected into a C-18 column (Agilent Prep – C18, 4.6 mm × 250 mm, 5 µm) with a mobile phase composed of acetonitrile and 5% acetic acid (80:20, v/v), running at a flow rate of 1 mL/min. Tamibarotene was detected at a wavelength of 280 nm with a retention time of 6.2 min. The measurements of drug content in each formulation were performed in triplicate. Drug content was calculated as the percentage of tamibarotene detected in the formulation to the total mass of powder.

2.2.6. Thermogravimetric analysis (TGA)

The residual moisture of the tamibarotene powders were determined using thermogravimetric analysis (TGA, TA Instruments, Newcastle, DE, USA). Approximately 3 to 5 mg of powder sample was loaded onto a titanium pan and kept at 25 °C until mass equilibrium was reached. The sample was heated to 120 °C at a constant rate of 10 °C/min. The amount of residual moisture was calculated as the change in powder mass upon heating.

2.2.7. Particle size distribution by laser diffraction

The volumetric size distribution of the dry powders was measured using a HELOS/KR laser diffractometer (Sympatec, Germany). For dispersion of the dry powder aerosols, a nasal powder device (Unit Dose System Powder Nasal Spray, Aptar Pharma, France) was filled with 2.0 ± 0.5 mg of powder and manually dispersed at a 30° angle with respect to the central unit (where the laser passes through). All measurements were conducted with 100 mm (R3) lens (measuring range 0.45–175 µm) with appropriate trigger and stop conditions, which correspond to optical concentrations above 0.5%. Particle size distribution was calculated using WINDOX 5 (Version 5.8.0.0) based on the enhanced Fraunhofer theory. The particle size data were expressed as D₁₀, D₅₀, and D₉₀, which represent the equivalent spherical volume diameters at 10%, 50% and 90% cumulative volumes, respectively. Span was calculated as (D₉₀ – D₁₀)/D₅₀. For each formulation, the most representative volumetric particle size distribution data were plotted on a graph for comparison.

2.2.8. Aerosol performance by Next Generation Impactor (NGI)

The aerodynamic size distribution of all powder formulations was evaluated using a Next Generation Impactor (NGI) coupled with a 1 L glass expansion chamber (Copley, Nottingham, UK). Before dispersion, a thin layer of silicon grease (LPS Laboratories, Illinois, GA, USA) was coated onto the stages of the NGI to reduce particle bounce and wall

losses. A powder mass of 3.0 ± 0.1 mg was loaded into a nasal powder device (Unit Dose System Powder Disposable Nasal Spray, Aptar Pharma, France) and dispersed at a 30° angle into the inlet hole (1 cm diameter) of the expansion chamber at a flow rate of 28.3 L/min (3.5 kPa pressure drop). The flow rate was varied at 15 and 40 L/min (1.2 and 7.5 kPa pressure drop, respectively) for measurement of mixed formulations, SFD-MIX-1 and SD-MIX-1. All dispersions were performed with 4 L of air drawn into the NGI. After each dispersion, methanol was used to rinse and dissolve all powder deposited on the stages of the NGI and expansion chamber. The collected samples were filtered through a 0.45- μ m membrane filter and analysed by HPLC. For each powder formulation, dispersions were performed in triplicates. The recovered dose was defined as the total mass of tamibarotene quantified on all stages of the NGI in a single run. Residual fraction (RF) referred to the fraction of powder that was undispersed and remained in the device. Nasal fraction (NF) was defined as the percentage fraction of particles that exited the dispersion device and had an aerodynamic diameter of over 10.0 μ m. Throat fraction (TF) was defined as the percentage of particles with aerodynamic diameter between 5.0 μ m and 10.0 μ m. Fine particle fraction (FPF) was defined as the percentage fraction of particles with aerodynamic diameter below 5.0 μ m. All fractions (RF, NF, TF and FPF) were calculated with respect to the recovered dose.

2.2.9. Dissolution study

Dissolution study was performed with the emitted fraction (EF) of the powder formulation, which is defined as the fraction of powder that exited the dispersion device. A 100 mL jacketed beaker containing 10 mL of simulated nasal fluid (SNF) (Trenkel and Scherliess, 2021) was used to examine the dissolution rate of the tamibarotene formulations prepared with the ultrasonic nozzle (SFD-USN and SD-USN) designed for nasal deposition (Supplementary Fig. S1A). The temperature was maintained at 37°C and the medium was stirred at 75 rpm with a magnetic bar. The EF of the nasal formulations were collected by a dosage unit sampling apparatus (DUSA, Copley Scientific, UK) after dispersion from the nasal powder device with a flow rate of 28.3 L/min. A powder mass of 2.0 ± 0.1 mg was dispersed, and the EF was collected on a glass fibre filter paper from the DUSA which was then transferred into the jacketed beaker and submerged in dissolution medium. At pre-determined time intervals, 0.5 mL of dissolution medium was withdrawn and filtered through a 0.45- μ m membrane filter before quantification by HPLC. After each sampling point, the medium was made up to 10 mL by replacing with an equal volume of pre-warmed fresh dissolution medium. For formulations prepared with the two-fluid nozzle (SFD-TFN and SD-TFN) designed for lung deposition, a 500 mL jacketed beaker containing 100 mL of simulated lung fluid (SLF) was used as the dissolution medium (Liao et al., 2021) (Supplementary Fig. S1B). The temperature was maintained at 37°C and the medium was stirred at 75 rpm with a magnetic bar. The EF of formulations SFD-TFN and SD-TFN were collected as described above and transferred to the jacketed beaker. At pre-determined time intervals, 1 mL of dissolution medium was withdrawn and filtered through 0.45 μ m membrane filter before quantification by HPLC. After each sampling point, the medium was made up to 100 mL by replacing with an equal volume of pre-warmed fresh dissolution medium. For comparison, the dissolution profile of equivalent amount of raw tamibarotene powder was studied in the simulated nasal and lung environment without dispersion. It is noted that due to the poor aqueous solubility of tamibarotene and the small volume of dissolution medium used to simulate the physiological condition, sink condition was not applied. All the dissolution tests were carried out in triplicates.

2.2.10. Differential scanning calorimetry

Differential scanning calorimetry (DSC) (DSC 250, TA Instruments, Newcastle, DE, USA) was used to investigate the thermal response of raw tamibarotene, the SFD and SD formulations and their physical mixtures. Approximately 1 mg of powder was weighed, loaded into hermetically

sealed aluminium pans, and heated from 50°C to 280°C at a constant rate of $10^\circ\text{C}/\text{min}$. The thermogram of each sample was obtained.

2.2.11. Statistical analysis

Statistical analyses were conducted using Prism 8.0 (GraphPad Software, La Jolla, CA, USA) for one-way ANOVA and Student's *t*-test. A significance level of $p = 0.05$ was used for all statistical analysis in this study.

3. Results

3.1. Drug content, production yield and residual moisture

The amount of tamibarotene present in the powder formulations was measured by HPLC (Table 2). In all the tested formulations, the measured drug content was close to the theoretical value of 30 % w/w of tamibarotene. For both SFD and SD techniques, the production yield varied with the nozzle used for atomization. The ultrasonic nozzle had a higher yield compared to the two-fluid nozzle, and SD had a lower yield compared to SFD (Table 2). All powder formulations demonstrated low levels of residual moisture ($<6\%$ w/w), although SD powder generally had a lower moisture content than SFD powder.

3.2. Particle size distribution

The volumetric particle size distribution of tamibarotene powder formulations was measured by laser diffraction after the powder was dispersed from a nasal powder device. The data were presented as incremental size distribution (Fig. 1), D_{10} D_{50} D_{90} and span (Table 3). Particles produced by SFD were generally larger than their SD counterparts. For both SFD and SD formulations, particles produced using the ultrasonic nozzle had a larger D_{50} as compared to those produced by the two-fluid nozzle. At 1:1 mixing ratio, the D_{50} of the mixed formulations (SFD-MIX-1 and SD-MIX-1) tended to be closer to the D_{50} of the smaller particle size formulation prepared with the two-fluid nozzle (SFD-TFN and SD-TFN, respectively). The mixed SFD and SD formulations were examined at several mixing ratios. A bimodal size distribution was observed in SD-MIX-0.25 and SD-MIX-1 formulations (at 3:1 and 1:1 of SD-USN : SD-TFN ratio, respectively), with each of the two separate peaks corresponding to the individual peaks of SD-USN and SD-TFN. When the proportion of SD-TFN increased in the mixed formulation, the peak corresponding to the smaller particle size increased while the peak corresponding to the larger particle size diminished. As the content of SD-TFN further increased (SD-MIX-3 and SD-MIX-7 at 1:3 and 1:7 of SD-USN : SD-TFN ratio, respectively), a unimodal distribution was observed with the mode similar to that of the SD-TFN formulation. In contrast, the SFD mixed formulations tended to have broader peak due to the wider distribution of particle size produced by SFD. When the proportion of SFD-TFN increased (SFD-MIX-2, SFD-MIX-3, and SFD-MIX-7 at 1:2, 1:3 and 1:7 of SFD-USN: SFD-TFN ratio, respectively), the magnitude of the peak increased and shifted to the left, indicating a

Table 2

Production yield, tamibarotene content and residual moisture of the spray freeze dried (SFD) and spray dried (SD) tamibarotene formulations. Drug content data are presented as mean (standard deviation), $n = 3$.

Formulation	Spray Freeze Drying			Spray Drying		
	SFD-USN	SFD-TFN	SFD-MIX-1	SD-USN	SD-TFN	SD-MIX-1
Production yield (% w/w)	93.5	71.4	N.A.	80.3	50.6	N.A.
Drug content (% w/w)	27.7 (0.3)	27.9 (1.3)	27.8 (0.5)	29.6 (0.5)	30.0 (3.5)	30.2 (1.1)
Residual moisture (% w/w)	5.1	5.5	N.A.	2.6	4.4	N.A.

N.A. Not applicable.

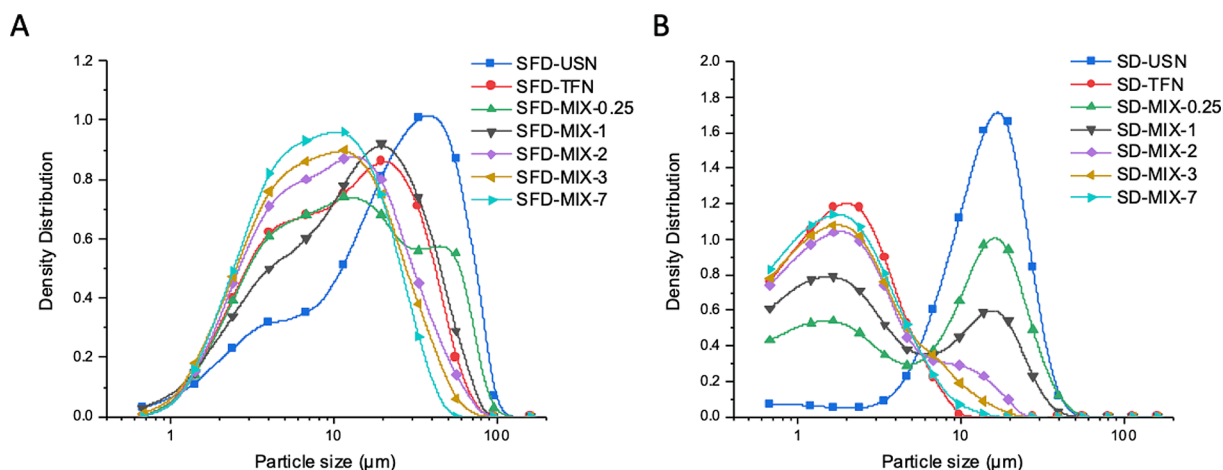


Fig. 1. Incremental particle size distribution of tamibarotene powder formulations. The powders were prepared by (A) spray freeze drying (SFD) and (B) spray drying (SD). The powders were dispersed using a nasal powder device and the volumetric diameter was measured by laser diffraction. For each formulation, the most representative volumetric particle size distribution data were plotted for comparison.

Table 3

Volumetric particle size distribution of tamibarotene powder formulations. The powders were dispersed using the nasal powder device and the particle size distribution was measured by laser diffraction. Data are presented as mean (standard deviation), $n = 3$.

	Volumetric diameter			
	D ₁₀ (μm)	D ₅₀ (μm)	D ₉₀ (μm)	Span
SFD-USN	3.26 (0.20)	21.75 (1.09)	59.85 (0.98)	2.61 (0.15)
SFD-TFN	2.70 (0.05)	11.68 (0.41)	37.95 (2.52)	3.02 (0.11)
SFD-MIX-0.25	2.67 (0.08)	10.81 (0.58)	47.59 (4.03)	4.17 (0.46)
SFD-MIX-1	2.60 (0.13)	11.24 (1.77)	33.54 (5.22)	2.75 (0.04)
SFD-MIX-2	2.54 (0.07)	8.47 (0.68)	25.40 (3.62)	2.69 (0.19)
SFD-MIX-3	2.45 (0.05)	8.57 (0.20)	25.29 (0.96)	2.67 (0.15)
SFD-MIX-7	2.52 (0.03)	8.63 (0.77)	24.95 (2.65)	2.60 (0.08)
SD-USN	5.27 (0.64)	13.42 (1.01)	24.89 (0.75)	1.47 (0.11)
SD-TFN	0.73 (0.03)	2.10 (0.41)	9.30 (7.30)	3.76 (2.50)
SD-MIX-0.25	0.89 (0.04)	7.25 (1.19)	22.21 (0.97)	2.99 (0.41)
SD-MIX-1	0.74 (0.02)	2.22 (0.30)	14.46 (3.13)	6.13 (0.65)
SD-MIX-2	0.71 (0.01)	1.83 (0.07)	7.13 (0.42)	3.51 (0.19)
SD-MIX-3	0.70 (0.01)	1.77 (0.07)	5.53 (0.18)	2.73 (0.11)
SD-MIX-7	0.69 (0.01)	1.66 (0.04)	4.17 (0.44)	2.09 (0.23)

larger proportion of smaller particles. SFD-MIX-0.25 formulation (3:1 of SFD-USN : SFD-TFN ratio) demonstrated a very broad distribution, implying a relatively even distribution of particle sizes.

3.3. Morphology

The morphology of the tamibarotene powder formulations were visualized by scanning electron microscopy (SEM) under $\times 2,500$ magnification (Fig. 2) to examine the particle surface properties and under $\times 500$ magnification (Supplementary Fig. S2) to provide the overall particle distribution. While unformulated tamibarotene exists as irregular rod-shaped crystalline structures, the SFD and SD powders were spherical. The surface of the SFD particles was slightly porous with visible cavities (at high magnification) as compared to the smooth exterior texture of the SD particles. The single formulations exhibited a relatively uniform size distribution. For both SFD and SD processes, the particles produced using the two-fluid nozzle were small ($<5 \mu\text{m}$) and seemed to aggregate as compared to the larger discrete particles produced by the ultrasonic nozzle ($>10 \mu\text{m}$). When two single formulations prepared with the same drying method but different nozzle were mixed at a 1:1 ratio (SFD-MIX-1 and SD-MIX-1), a blend of small and large particles can be clearly observed, displaying two distinct particle sizes. Most of the particles retained their spherical structures after mixing,

with some of the smaller particles loosely attached to the surface of the larger particles. Some small fragments can also be seen deposited on the surface of the particles after mixing, further broadening the dual particle size distribution in the mixed formulation. The mixed formulations with different mixing ratio showed distinctly different distributions of particles. When high proportion of SFD-USN or SD-USN was present in the mixed formulation (SFD-MIX-0.25, SD-MIX-0.25), large particles ($>10 \mu\text{m}$) were the dominant species, with smaller particles on the surface and in the surrounding. As the proportion of SFD-TFN or SD-TFN increased, there were fewer large particles and increasingly more smaller particles ($<10 \mu\text{m}$), as clearly shown in SFD-MIX-7 and SD-MIX-7.

3.4. Aerosol performance

Suitable range of aerodynamic diameter of the dispersed particles is required for efficient deposition to the appropriate sites along the respiratory tract. The aerosol performance of the tamibarotene powder formulations is presented as RF, NF, TF and FPF which were obtained from the NGI experiments (Fig. 3A and 3B). All formulations demonstrated excellent dispersion from the nasal device (RF $<10\%$). The formulations produced with the ultrasonic nozzle, SFD-USN and SD-USN exhibited high NF (both over 80%) and low FPF (both below 10%), suggesting high nasal deposition and low lung deposition. In comparison, aerosol performance of formulations prepared with the two-fluid nozzle exhibited moderate FPF, with 34% for SFD-TFN and 44% for SD-TFN when dispersed with a nasal powder device, indicating the feasibility for lung deposition through intranasal administration.

The rationale of the mixed formulations was to allow the manipulation of NF and FPF by varying the ratio between USN and TFN formulations. All mixed formulations showed similarly low RF and TF regardless of the mixing ratio, demonstrating that the mixed dry powder formulations were dispersed and aerosolized effectively from the nasal powder device, with minimal powder deposition at unintended sites. When mixed at a 1:1 ratio, the NF and FPF values of both SFD-MIX-1 and SD-MIX-1 were close to the average of the individual formulations, achieving a NF:FPF ratio of approximately 71:23 and 70:25, respectively. When a wider range of mixing ratio was investigated, a linear trend for the ratio of NF:FPF was observed (Fig. 3C and 3D). As the percentage of SFD-TFN or SD-TFN increased in the mixed formulation, FPF increased proportionally until the maximum FPF (32% and 38%, respectively) was reached, while the NF decreased to the minimum value (59% and 55%, respectively). The NF:FPF ratio of the SD-MIX formulations exhibited a wider range from 85:11 (SD-MIX-0.25) to 55:38 (SD-MIX-7) as compared to the SFD-MIX formulations with a

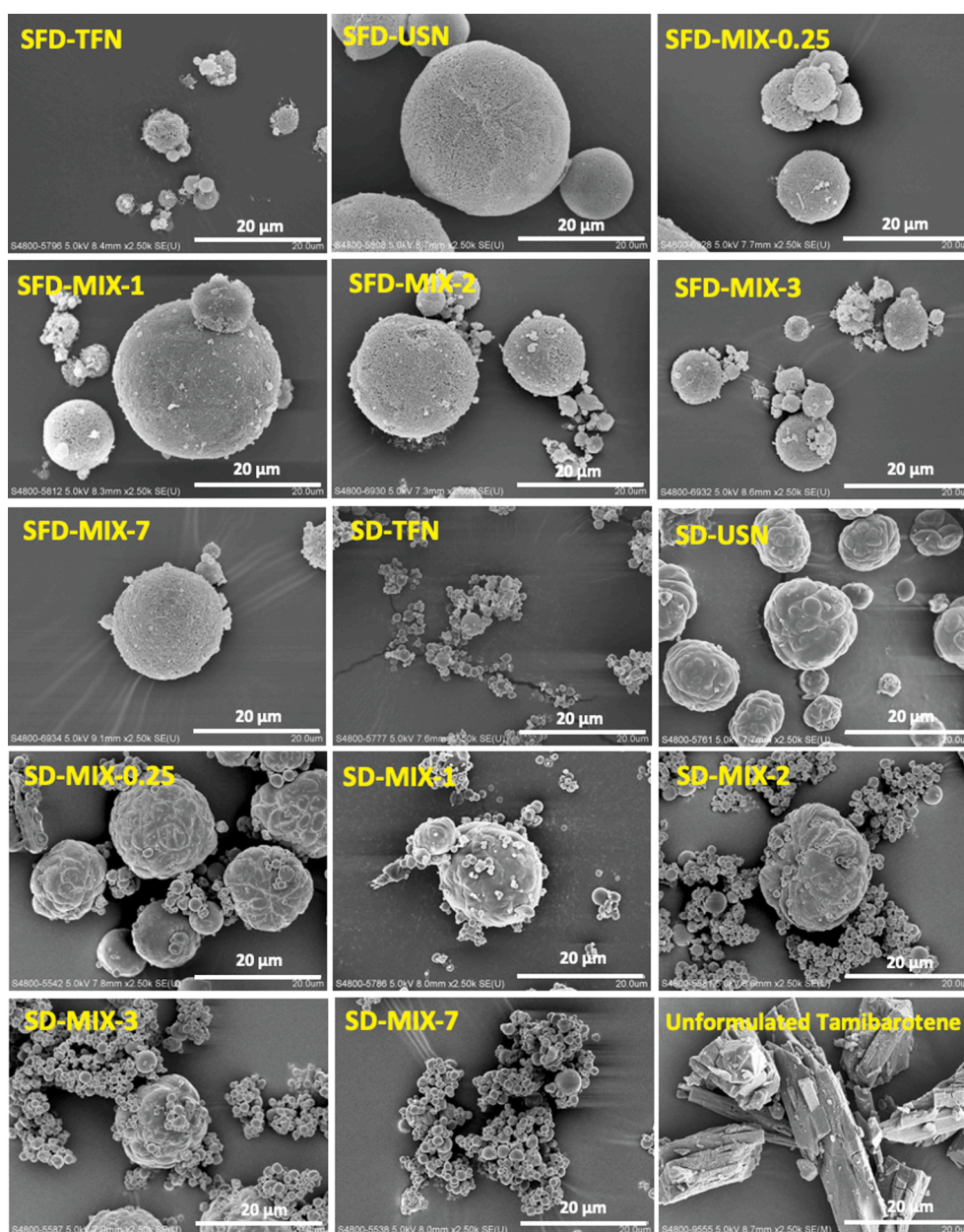


Fig. 2. Scanning electron microscopy (SEM) images of tamibarotene formulations at high magnification. The powders were prepared by spray freeze drying (SFD) and spray drying (SD). Unformulated tamibarotene was included for comparison. The SEM images were observed under $\times 2,500$ magnification, scale bar = 20 μm ; TFN – two-fluid nozzle; USN – ultrasonic nozzle.

range from 78:17 (SFD-MIX-0.25) to 59:32 (SFD-MIX-7).

To further investigate the effect of flow rate on powder deposition, the aerosol performance of two mixed formulations SFD-MIX-1 (Fig. 4A) and SD-MIX-1 (Fig. 4B) were examined at three different flow rates (15, 28.3 and 40 L/min) with powders dispersed from a nasal device. The NF and PPF were compared using one-way ANOVA (Supplementary Table S1). For both formulations, the aerosol performance at different flow rates were significantly different ($p < 0.05$). While RF and TF remained the same, NF decreased at a higher flow rate, with a corresponding increase in PPF. In our previous study, SFD powder of tamibarotene prepared with the two-fluid nozzle was reported to be suitable for targeting the respiratory tract when aerosolized with the Breezhaler (Liao et al., 2021). In comparison with the nasal device, SFD-TFN dispersed by the Breezhaler (for oral inhalation) exhibited significantly higher PPF ($p < 0.05$) (Supplementary Fig. S3A). There was no significant change in aerosol performance of SFD-TFN when Breezhaler

was operated at 60 and 90 L/min. In contrast, the PPF of SD-TFN was not significantly different regardless of the dispersion device and flow rate used for dispersion (Supplementary Fig. S3B). However, the RF of SD-TFN significantly increased when dispersed from the Breezhaler, implying inefficient dispersion. Using the Handihaler with a higher resistance and different mechanism of dispersion improved powder dispersion, showing a reduction in RF.

3.5. Dissolution profile

Dissolution study was performed using the EF of the tamibarotene powder formulations. The powders were dispersed using the nasal powder device and collected from the DUSA. Formulations prepared with ultrasonic nozzle (SFD-USN and SD-USN) were designed for nasal deposition and were evaluated in SNF (Fig. 5A), while formulations prepared with the two-fluid nozzle (SFD-TFN and SD-TFN) were

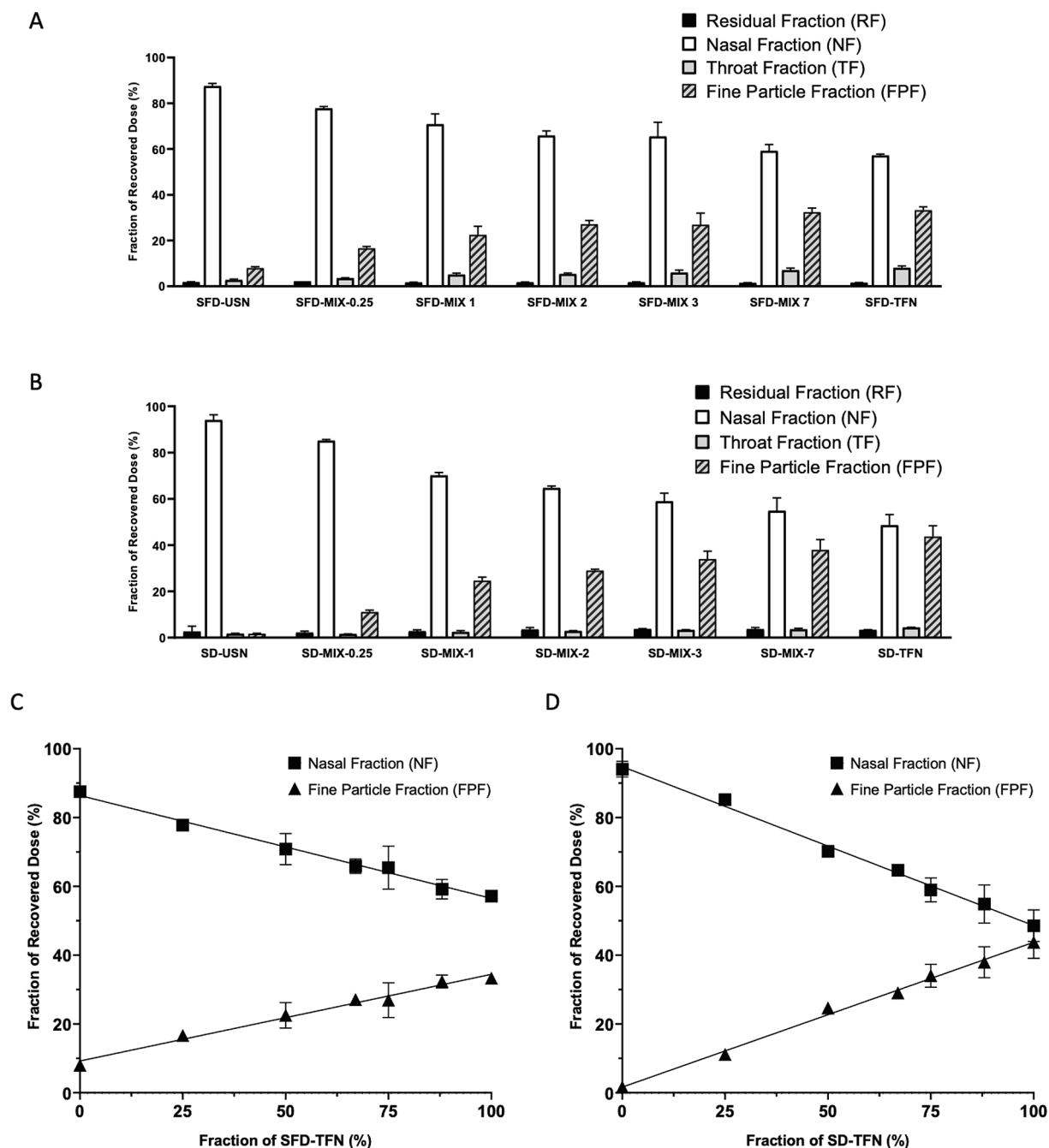


Fig. 3. Aerosol performance of tamibarotene powder formulations dispersed from nasal device operated at a flow rate of 28.3 L/min. The formulations were evaluated by Next Generation Impactor (NGI) coupled with 1 L glass expansion chamber. (A & C) Spray freeze dried powder formulations prepared with ultrasonic nozzle (SFD-USN) and two-fluid nozzle (SFD-TFN) at different mixing ratios; (B & D) spray dried powder formulations prepared with ultrasonic nozzle (SD-USN) and two-fluid nozzle (SD-TFN) at different mixing ratios. Residual fraction (RF), nasal fraction (NF), throat fraction (TF) and fine particle fraction (FPF) were expressed as the percentage by mass of tamibarotene with respect to the recovered dose (A & B). Linear regression of NF and FPF was plotted against fraction of SFD-TFN (C) and SD-TFN (D) in the formulation. Data were presented as mean \pm standard deviation ($n = 3$).

designed for pulmonary deposition and were evaluated in SLF (Fig. 5B) for their dissolution profile. All the tamibarotene powder formulations demonstrated burst-release profiles with a faster dissolution rate compared to unformulated tamibarotene. For formulations prepared with the ultrasonic nozzle (for nasal deposition), more than 50% of tamibarotene in SD-USN was dissolved in 1 h while just over 30% of the drug in SFD-USN was dissolved in 2 h. The cumulative concentration of both formulations stabilized to around 40% after 4 h. At the end of the experiment (24 h), a significantly higher amount of tamibarotene (40%) was released from SD-USN compared to the unformulated tamibarotene

(Student's t -test, $p < 0.01$). In comparison, the unformulated tamibarotene exhibited a slower rate of dissolution until the end of the experiment. For formulations prepared with the two-fluid nozzle (for lung deposition), more than 50% of tamibarotene in SD-TFN formulation was dissolved within the first 15 min. In contrast, SFD-TFN dissolved at a faster rate, reaching a maximum of more than 60% of tamibarotene released within the first 5 min. After reaching the peak concentration, there was a slight decrease in the drug concentration of both formulations. The cumulative concentration remained relatively constant for the next 6 h, with about 60% of drug dissolved at the end of the experiment

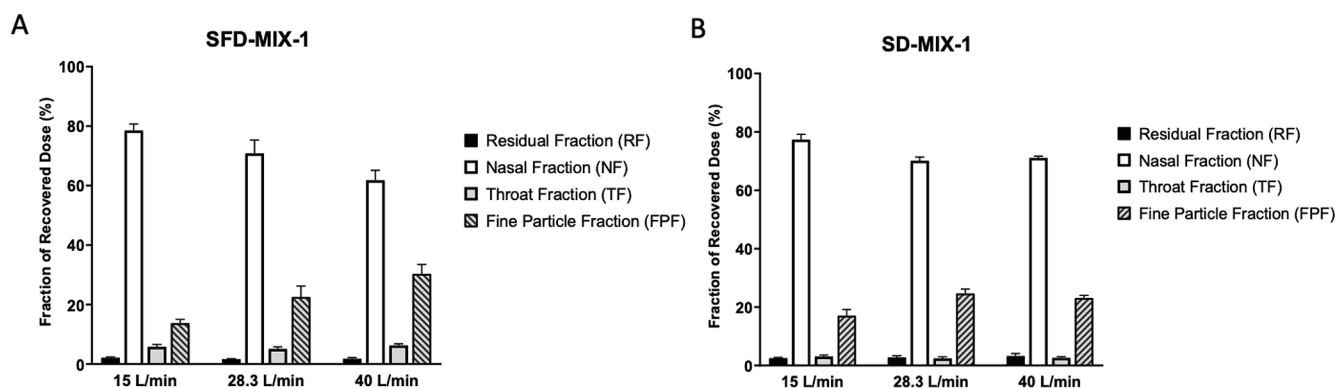


Fig. 4. Aerosol performance of tamibarotene powder formulations dispersed from nasal device at different flow rates. (A) Spray freeze dried powder formulation (SFD-MIX-1) and (B) spray dried powder formulation (SD-MIX-1) were evaluated by Next Generation Impactor (NGI) coupled with 1 L glass expansion chamber and nasal device operated at 15, 28.3 and 40 L/min. Residual fraction (RF), nasal fraction (NF), throat fraction (TF) and fine particle fraction (FPF) were expressed as the percentage by mass of tamibarotene with respect to the recovered dose. Data were presented as mean \pm standard deviation ($n = 3$).

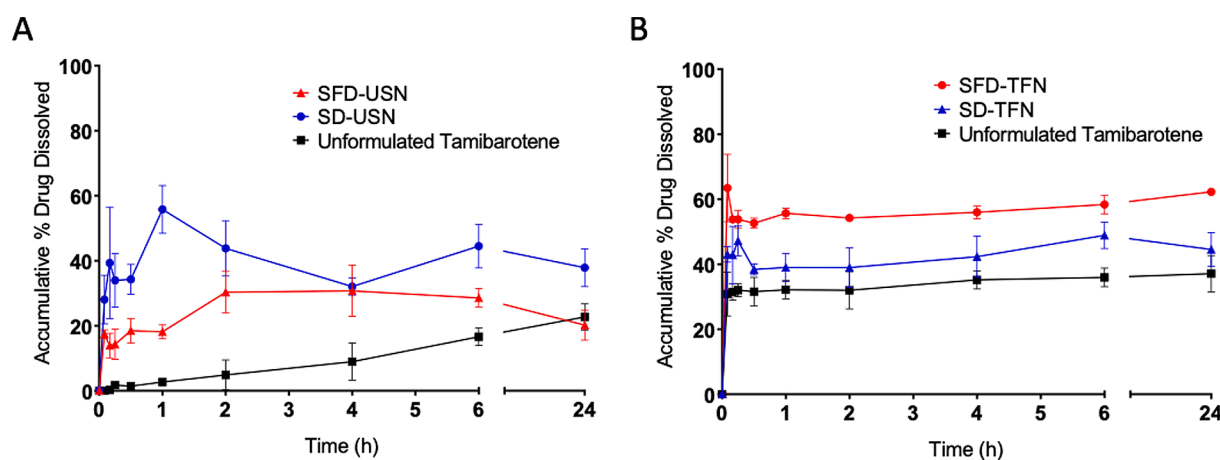


Fig. 5. Dissolution profiles of the emitted fraction (EF) of tamibarotene powder formulations. The EF was collected from a dosage unit sampling apparatus (DUSA) after dispersion from the nasal powder device. The dissolution was performed at 37 °C in (A) 10 mL of simulated nasal fluid and (B) 100 mL simulated lung fluid for up to 24 h. Unformulated tamibarotene was used as comparison. Data were presented as mean \pm standard deviation ($n = 3$).

(24 h). In SLF, the unformulated tamibarotene dissolved at a slower rate with significantly lower amount of drug dissolved (30%) compared to SFD-TFN after 24 h (Student's t -test, $p < 0.01$).

3.6. Powder crystallinity

The crystallinity of raw drug, excipient and the tamibarotene powder formulations were examined using the DSC (Fig. 6). In the DSC thermogram of raw unformulated tamibarotene, the two endothermic peaks suggest an initial change in crystalline state at 184 °C and a subsequent breakdown of the re-crystallized form at 231 °C, which corresponds to the melting point of tamibarotene. The excipient HPBCD was amorphous as no significant thermal event was detected. Upon physical mixture of raw tamibarotene with HPBCD, the endothermic peaks can still be detected at the same temperatures (184 °C and 231 °C). This suggests that raw tamibarotene retained its crystalline state in a physical mixture with HPBCD. After SFD and SD, the formulations became amorphous as shown in their respective thermograms with no significant thermal events.

4. Discussion

Delivery of a broad-spectrum antiviral agent to the upper and lower respiratory tract simultaneously could potentially improve the treatment efficacy of respiratory viral infections, especially those caused by

previously unknown viruses. For local drug delivery to the respiratory tract, the drug is usually delivered either to the nasal tract through the intranasal administration, or to the lung through inhalation. No current drug delivery system can target both nasal cavity and respiratory region in a single formulation other than systemic delivery, in which higher dose and toxicity are expected. This study explored both SFD and SD technology to produce tamibarotene powder formulations with dual targeting property. In addition, the deposition characteristics can be easily manipulated, enabling the drug to be deposited at the appropriate dose to the infected sites. This could be achieved by blending powder with two distinct particle sizes at an appropriate ratio. After powder production by SFD or SD, the single formulations were mixed with the Turbula® shaker-mixer type T2F. This laboratory scale mixer applies the powder blending principles of rotation, translation and inversion (Porion et al., 2000). The powders are mixed within the cylindrical mixing chamber with an alternating and rhythmic motion to achieve blending. When mixing particles that are not similar in particle size, it is often difficult to achieve a homogenous mixture with two-dimensional mixers with a single axis of rotation due to radial and axial segregation of powders (Hill et al., 1997). As we aimed to develop a powder mixture with particles of different size and density, a three-dimensional (3D) periodic mixer was used, which allows 3D movement of particles with different sizes to achieve good mixing at high rotational speed and number of rotations (Marigo et al., 2011; Sommier et al., 2001). When mixing the different powder formulations, SFD powders were observed

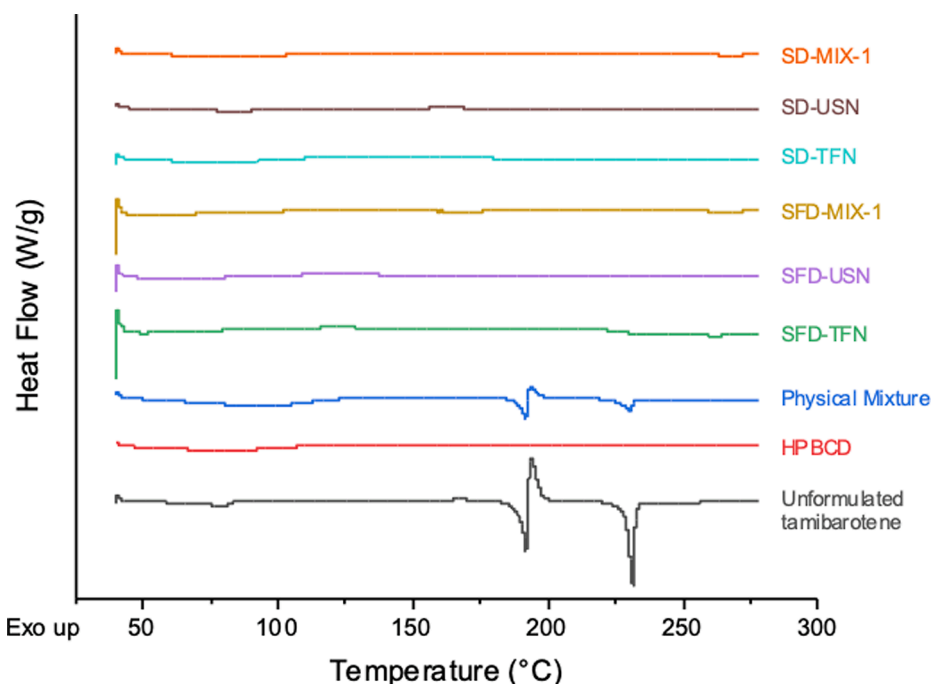


Fig. 6. Differential scanning calorimetry (DSC) thermograms of tamibarotene powder formulations. The thermograms of spray freeze dried (SFD) and spray dried (SD) powder formulations of tamibarotene. Unformulated tamibarotene, HPBCD and physical mixture of unformulated tamibarotene and HPBCD were used as comparison. Negative peak in DSC thermogram represents endothermic events.

to be more flowable as compared to SD, possibly due to the larger physical size as demonstrated in measurement by laser diffraction and SEM images (Liang et al., 2018). The mixing process was ensured to be sufficiently uniform as each powder formulation showed highly similar aerosol and physicochemical characteristics on repeated measurement.

For the treatment of respiratory viral infections, the nasal cavity and the deep lung region are the two specific sites that the dual targeting formulations of tamibarotene are aimed at. The aerosol performance of a good dual targeting powder formulation should have a NF (for nasal deposition) and FPF (for lung deposition) in an appropriate ratio. As viral infections such as COVID-19 affect both the upper and lower respiratory tract, it is crucial that high doses of the antiviral drug can reach both infected sites to achieve maximal therapeutic effect. When dispersed by the nasal powder device, both SFD and SD formulations demonstrated low RF which indicated good powder dispersion from the device. The single formulations prepared with the ultrasonic nozzle and two-fluid nozzle exhibited high aerosol deposition at their specified target sites, i.e., the nasal cavity and the lung, respectively. At 1:1 mixing ratio, the results from aerosol characterization suggest that the dual targeting formulation enable efficient powder deposition in both the upper and lower airways. The fraction of particles deposited in the throat was minimal and there were two major fractions of the formulation that deposit separately in the nasal (NF) and lung region (FPF). This dual deposition characteristic is also supported by the incremental volumetric particle size distribution, especially with SD formulations which showed two distinct peaks after mixing, corresponding to the two particle size ranges of the single formulations. The SEM images also reveal an observable mixture of large and small particles in a well distributed manner.

To further investigate the manipulation of bimodal deposition distribution, different mixing ratios of powder prepared using the ultrasonic nozzle and two-fluid nozzle were used to examine how varying the ratio may affect the deposition profile of the mixed formulations. Aerosol performance study showed that the ratio of NF:FPF varied linearly with the mixing ratio for both SFD and SD powder formulations. As the proportion of TFN formulation increased in the mixture, the FPF increased proportionally until the maximum FPF that was approximate

to the single TFN formulation was reached. Similarly, particle size measurement by laser diffraction showed that the peak height corresponding to the lower particle size range increased as the proportion of TFN increased in the formulation. For the larger particles intended for nasal deposition, aerosol characterisation showed that NF increased as the proportion of USN formulation increased in the mixture. The SEM images also showed significantly more large particles that may have resulted in the increased fraction of particles within the nasal size range ($>10\ \mu\text{m}$). As the content of TFN formulation in the mixture increased, the NF decreased proportionally. Overall, the mixing ratio may potentially be manipulated to tailor the ratio of NF:FPF in the mixed formulation for customizable aerosol deposition profile in the nasal cavity and the lung.

When the aerosol performance of SFD-MIX-1 and SD-MIX-1 were tested at different flow rates (15, 28.3 and 40 L/min), which were chosen based on the normal nasal breathing of 20 to 30 L/min of an adult (Djupesland, 2013). RF remained low, demonstrating excellent dispersion from the nasal powder device. This could be due to the Aptar Unit Dose Powder system being an active (hand-actuated) nasal insufflator, which adopts a mechanism other than the patient's inspiration effort to disperse the powder. However, the aerosol performance of SFD-MIX-1 was affected by the flow rate used. As SFD particles are porous and fragile, fragmentation of the larger particles could have caused a higher FPF at a higher flow rate. In contrast, NF was higher at a lower flow rate, possibly due to increased sedimentation and deposition in the nasal region. For dry powder delivery to the respiratory tract, the aerosol deposition profile should ideally be minimally affected by the patient's inspiratory flow rate. The deposition fractions should be independent of the flow rate to achieve the intended therapeutic dose at the target sites in a reproducible manner. In this aspect, the aerosol performance of the SD particles was less affected by the flow rate and the SD formulation would display the appropriate dual deposition characteristic for targeted drug delivery. Nonetheless, patients may need to control their nasal breathing pattern during powder dispersion, similar to the use of metered dose inhaler for oral inhalation, to achieve a reproducible powder deposition profile for both formulations.

In our previous study, SFD powder of tamibarotene prepared with

the two-fluid nozzle was reported to be suitable for targeting the respiratory tract when aerosolized with Breezhaler (Liao et al., 2021). The FPF was significantly higher when SFD-TFN was dispersed with the Breezhaler when compared with the nasal device. The lower FPF when dispersed from the nasal device may have limited the NF:FPF range of the mixed formulations. To achieve maximum deposition into the lung when nasal deposition is not required, dry powders should be orally inhaled with an inhaler instead. While the FPF of SD-TFN was unaffected by the inhaler device and flow rate used for dispersion, the RF was higher when the Breezhaler was used for dispersion. The RF in the Breezhaler remained significantly higher even at higher flow rates, demonstrating inefficient dispersion of the SD formulation, possibly due to the high level of aggregation of the small particles. By using the Handihaler, which has a different mechanism of dispersion from the Breezhaler, the RF was lower but still significantly higher compared to dispersion from nasal device. In this context, the SD formulation could be more compatible with the nasal device for drug delivery to the lungs. If the FPF of SD-TFN can be further increased (for example, by decreasing the aerodynamic diameter of the particles), the NF:FPF range of the mixed formulations may potentially be broadened.

To overcome the poor aqueous solubility of tamibarotene, TBA and ethanol were used as co-solvents in the feed solution for SFD and SD, respectively, with HPBCD used as excipient (Jacob and Nair, 2018; Lo et al., 2021). The sublimation of the frozen TBA crystals during freeze drying resulted in the formation of pores that could be seen in SFD powders. In contrast, SD powders produced in the presence of ethanol had a smooth exterior surface due to the rapid evaporation of the solvent during spray drying at high temperature. TBA and ethanol were chosen as co-solvents as they are widely used in SFD and SD and considered low toxicity and generally safe for use in inhalation formulation (McGregor, 2010). All SFD and SD formulations demonstrated low levels of residual moisture in the powders. Improving the dissolution profile of tamibarotene is another key feature of the SFD and SD formulations, as drug solubility was improved by producing amorphous solid dispersions of tamibarotene. Good aqueous solubility is important to ensure dissolution of drug to achieve antiviral effect at the site of deposition. Dissolution studies were conducted to compare the drug release profile of the SFD and SD powder formulations in simulated nasal and lung environments. As only powder that can be dispersed from the nasal device could reach the nasal and lung regions, the EF was collected by the DUSA for the dissolution test. Both SFD and SD formulations demonstrated rapid dissolution and a burst-release profile. The improved dissolution profile can be explained by the HPBCD inclusion complex formed with tamibarotene through hydrophobic interaction. By incorporating tamibarotene into the hydrophobic internal cavity, HPBCD improved drug solubility with its hydrophilic external surface. The DSC thermograms further confirmed the amorphous state of the SFD and SD formulations which enhanced the dissolution rate as compared to the crystalline unformulated tamibarotene. The dissolution profile is also affected by the mechanism involved in the drug release from HPBCD inclusion complexes which is a dynamic process (Stella et al., 1999). The burst-release profile of the formulations may be attributed to the spontaneous release followed by subsequent recrystallization due to supersaturation in the dissolution medium. While this dissolution profile allows rapid onset of antiviral action at the target sites, additional methods to prolong nasal and pulmonary retention time may be required. For the nasal formulations, SD-USN has faster dissolution time compared to SD-TFN, possibly due to the smaller particle size of SD-USN and resultant higher surface area for hydration. For the pulmonary formulations, SFD-TFN demonstrated a larger amount of drug dissolved compared to SD-TFN, possibly due to its higher porosity which allowed more drug to be in contact with the medium. Due to the different dissolution experimental set up, the amount of drug dissolved in the simulated lung environment (500 mL SLF) was significantly higher than in the simulated nasal environment (10 mL SNF), possibly due to saturation and reaching the maximum solubility of tamibarotene in the media. Overall, the enhanced solubility

and dissolution profile is crucial for local therapeutic action and absorption of the tamibarotene dry powder formulations after efficient deposition at the targeted nasal and lung regions.

This study provided a proof-of-concept that dual targeting in the respiratory tract could be achieved by blending powders of two particle size ranges, with potential application in the treatment of respiratory viral infections using a handheld nasal powder device. However, it is important to acknowledge some limitations of this study, and the challenges to be overcome in order to move this formulation strategy forward. First, the *in vitro* aerosol performance of the powder formulations was the focus of this study to examine their deposition profile in various conditions of powder dispersion. It is necessary to ensure that the particles can escape entrapment by the nasal mucus and evade mucociliary clearance in the nasal cavity to reach their target sites (Tiozzo Fasiolo et al., 2018). Additional excipients such as mucoadhesive agent may be required in the nasal fraction to prolong residence time in the nasal cavity (Illum, 2012). Second, it is crucial to understand the deposition mechanisms of particles with bimodal size distribution through the nasal route and the interaction (e.g., agglomeration) between particles of different size, which may affect regional deposition within the nasal cavity (Nizic Nodilo et al., 2021). Further investigation of mixing process may also be required to understand the mixing mechanism, powder segregation and optimal mixing parameters for the polydisperse powders at different powder mixing ratios. Moreover, it would be interesting to explore the potential of whole lung deposition (rather than focusing on two particular regions in the airways) which will require more sophisticated approach such as three dimensional lung models or computational modelling to examine particle deposition profile. The dual targeting formulation can be potentially applied not only to antiviral agents, but other therapeutics that are required to be delivered to both the nasal and respiratory tracts such as neutralizing antibodies (Halwe et al., 2021; Piepenbrink et al., 2021), vaccines (An et al., 2021; Heida et al., 2021) and other antimicrobial agents. In order to make this formulation strategy clinically relevant, it is important to know the dose required at each site of action in the first place so that a suitable formulation can be tailor-made accordingly.

5. Conclusion

Dual targeting powder formulation of tamibarotene was successfully prepared by SFD and SD, for simultaneous nasal and pulmonary delivery using a nasal powder device for insufflation. By varying the mixing ratio of tamibarotene powder produced by ultrasonic nozzle and two-fluid nozzle, two distinct fractions of particle sizes ranges could potentially be modified to tailor aerosol deposition fractions in the nasal cavity and pulmonary region. The powder blend demonstrated bimodal size distribution, effective aerosol deposition profile and improved dissolution rate. SD is preferred over SFD as the formulation method for tamibarotene due to the superior powder characteristics (wider NF:FPF ratio and less flow-rate dependent aerosol performance) as well as practicality and scalability in pharmaceutical manufacturing. In this study, we reformulated a broad-spectrum antiviral drug, tamibarotene, that can be repurposed for prophylaxis and treatment of SARS-CoV-2 and/or coinfections with seasonal influenza A. This novel dual targeting powder formulation approach demonstrates a promising new platform for drug delivery of therapeutic agents such as neutralizing antibodies and vaccines for the treatment and prevention of respiratory viral infections.

CRedit authorship contribution statement

Han Cong Seow: Conceptualization, Methodology, Formal analysis, Investigation, Writing – original draft. **Qiuying Liao:** Methodology, Investigation. **Andy T.Y. Lau:** Formal analysis, Investigation. **Susan W. S. Leung:** Writing – review & editing, Resources, Funding acquisition. **Shuofeng Yuan:** Writing – review & editing, Resources, Funding acquisition. **Jenny K.W. Lam:** Conceptualization, Methodology,

Validation, Project administration, Resources, Writing – review & editing, Supervision, Funding acquisition.

Declaration of Competing Interest

The authors declare that they have no known competing financial interests or personal relationships that could have appeared to influence the work reported in this paper.

Acknowledgements

The study was financially supported by the Health and Medical Fund (HMRF 20190582, 19180502), Food and Health Bureau; the Health@InnoHK program of the Innovation and Technology Commission of the Hong Kong SAR Government; and the Seed Funding for Strategic Interdisciplinary Research Scheme, The University of Hong Kong. The authors thank Professor Kwok-Yung Yuen (Department of Microbiology, HKU) for his inspiration of this project, and Mr. Ray Lee (Department of Pharmacology and Pharmacy, HKU) for his kind assistance with the NGI and TGA experiments.

Appendix A. Supplementary data

Supplementary data to this article can be found online at <https://doi.org/10.1016/j.ijpharm.2022.121704>.

References

- An, X., Martinez-Paniagua, M., Rezvan, A., Sefat, S.R., Fathi, M., Singh, S., Biswas, S., Pourpak, M., Yee, C., Liu, X., Varadarajan, N., 2021. Single-dose intranasal vaccination elicits systemic and mucosal immunity against SARS-CoV-2. Single-dose intranasal vaccination elicits systemic and mucosal immunity against SARS-CoV-2. *iScience* 24 (9), 103037. <https://doi.org/10.1016/j.isci.2021.103037>.
- Baig, A.M., 2021. Targeting Neuroinvasion by SARS-CoV-2: Emerging Trends in Drug and Antibody Delivery to Combat COVID-19. *ACS Chem Neurosci* 12 (14), 2555–2557. <https://doi.org/10.1021/acchemneuro.1c00372>.
- de Vries, R.D., Schmitz, K.S., Bovier, F.T., Predella, C., Khao, J., Noack, D., Haagmans, B. L., Herfst, S., Stearns, K.N., Drew-Bear, J., Biswas, S., Rockx, B., McGill, G., Dorrello, N.V., Gellman, S.H., Alabi, C.A., de Swart, R.L., Moscona, A., Porotto, M., 2021. Intranasal fusion inhibitory lipopeptide prevents direct-contact SARS-CoV-2 transmission in ferrets. *Science* 371 (6536), 1379–1382. <https://doi.org/10.1126/science.abb4896>.
- Djupesland, P.G., 2013. Nasal drug delivery devices: characteristics and performance in a clinical perspective—a review. *Drug Deliv Transl Res* 3 (1), 42–62. <https://doi.org/10.1007/s13346-012-0108-9>.
- Emami, F., Vatanara, A., Park, E.J., Na, D.H., 2018. Drying Technologies for the Stability and Bioavailability of Biopharmaceuticals. *Pharmaceutics* 10 (3), 131. <https://doi.org/10.3390/pharmaceutics10030131>.
- Halwe, S., Kupke, A., Vanshylla, K., Liberta, F., Gruell, H., Zehner, M., Rohde, C., Krähling, V., Gellhorn Serra, M., Kreer, C., Klüver, M., Sauerhering, L., Schmidt, J., Cai, Z., Han, F., Young, D., Yang, G., Widera, M., Koch, M., Werner, A., Kämper, L., Becker, N., Marlow, M.S., Eickmann, M., Ciesek, S., Schiele, F., Klein, F., Becker, S., 2021. Intranasal Administration of a Monoclonal Neutralizing Antibody Protects Mice against SARS-CoV-2 Infection. *Viruses* 13 (8), 1498. <https://doi.org/10.3390/v13081498>.
- Heida, R., Hinrichs, W.L., Frijlink, H.W., 2021. Inhaled vaccine delivery in the combat against respiratory viruses: a 2021 overview of recent developments and implications for COVID-19. *Expert Rev Vaccines* 1–18. <https://doi.org/10.1080/14760584.2021.1903878>.
- Hill, K.M., Caprihan, A., Kakalios, J., 1997. Axial segregation of granular media rotated in a drum mixer: Pattern evolution. *Phys Rev E* 56 (4), 4386–4393. <https://doi.org/10.1103/PhysRevE.56.4386>.
- Hou, Y.J., Okuda, K., Edwards, C.E., Martinez, D.R., Asakura, T., Dinnon 3rd, K.H., Kato, T., Lee, R.E., Yount, B.L., Mascenik, T.M., Chen, G., Olivier, K.N., Ghio, A., Tse, L.V., Leist, S.R., Gralinski, L.E., Schafer, A., Dang, H., Gilmore, R., Nakano, S., Sun, L., Fulcher, M.L., Livraghi-Buttrico, A., Nicely, N.L., Cameron, M., Cameron, C., Kelvin, D.J., de Silva, A., Margolis, D.M., Markmann, A., Bartelt, L., Zumwalt, R., Martinez, F.J., Salvatore, S.P., Borczuk, A., Tata, P.R., Sontake, V., Kimple, A., Jaspers, I., O'Neal, W.K., Randell, S.H., Boucher, R.C., Baric, R.S., 2020. SARS-CoV-2 Reverse Genetics Reveals a Variable Infection Gradient in the Respiratory Tract. *Cell* 182 (2), 429–446. <https://doi.org/10.1016/j.cell.2020.05.042>.
- Illum, L., 2012. Nasal drug delivery - recent developments and future prospects. *J Control Release* 161 (2), 254–263. <https://doi.org/10.1016/j.jconrel.2012.01.024>.
- Jacob, S., Nair, A.B., 2018. Cyclodextrin complexes: Perspective from drug delivery and formulation. *Drug Dev Res* 79 (5), 201–217. <https://doi.org/10.1002/ddr.21452>.
- Jansook, P., Ogawa, N., Loftsson, T., 2018. Cyclodextrins: structure, physicochemical properties and pharmaceutical applications. *Int J Pharm* 535 (1–2), 272–284. <https://doi.org/10.1016/j.ijpharm.2017.11.018>.
- Kim, D.H., Lee, S.E., Pyo, Y.C., Tran, P., Park, J.S., 2020. Solubility enhancement and application of cyclodextrins in local drug delivery. *J Pharm Invest* 50 (1), 17–27. <https://doi.org/10.1007/s40005-019-00434-2>.
- Leung, S.S.Y., Parumasivam, T., Gao, F.G., Carrigy, N.B., Vehring, R., Finlay, W.H., Morales, S., Britton, W.J., Kutter, E., Chan, H.K., 2016. Production of Inhalation Phase Powders Using Spray Freeze Drying and Spray Drying Techniques for Treatment of Respiratory Infections. *Pharm Res-Dordr* 33 (6), 1486–1496. <https://doi.org/10.1007/s11095-016-1892-6>.
- Liang, W.L., Chan, A.Y.L., Chow, M.Y.T., Lo, F.F.K., Qiu, Y.S., Kwok, P.C.L., Lam, J.K.W., 2018. Spray freeze drying of small nucleic acids as inhaled powder for pulmonary delivery. *Asian J Pharm Sci* 13 (2), 163–172. <https://doi.org/10.1016/j.ajps.2017.10.002>.
- Liao, Q., Yip, L., Chow, M.Y.T., Chow, S.F., Chan, H.K., Kwok, P.C.L., Lam, J.K.W., 2019. Porous and highly dispersible voriconazole dry powders produced by spray freeze drying for pulmonary delivery with efficient lung deposition. *Int J Pharm* 560, 144–154. <https://doi.org/10.1016/j.ijpharm.2019.01.057>.
- Liao, Q., Lam, I.C.H., Lin, H.H.S., Wan, L.T.L., Lo, J.C.K., Tai, W., Kwok, P.C.L., Lam, J.K.W., 2020. Effect of formulation and inhaler parameters on the dispersion of spray freeze dried voriconazole particles. *Int J Pharm* 584, 119444. <https://doi.org/10.1016/j.ijpharm.2020.119444>.
- Liao, Q., Yuan, S., Cao, J., Tang, K., Qiu, Y., Seow, H.C., Man, R.-H., Shao, Z., Huang, Y., Liang, R., Chan, J.-W., Yuen, K.-Y., Lam, J.-W., 2021. Inhaled Dry Powder Formulation of Tamibarotene, a Broad-Spectrum Antiviral against Respiratory Viruses Including SARS-CoV-2 and Influenza Virus. *Adv Ther-Germany* 4 (7), 2100059. <https://doi.org/10.1002/adtp.v4.710.1002/adtp.202100059>.
- Liu, Y., Ning, Z., Chen, Y., Guo, M., Liu, Y., Gali, N.K., Sun, L., Duan, Y., Cai, J., Westerdahl, D., Liu, X., Xu, K., Ho, K.F., Kan, H., Fu, Q., Lan, K., 2020. Aerodynamic analysis of SARS-CoV-2 in two Wuhan hospitals. *Nature* 582 (7813), 557–560. <https://doi.org/10.1038/s41586-020-2271-3>.
- Lo, J.C.K., Pan, H.W., Lam, J.K.W., 2021. Inhalable Protein Powder Prepared by Spray-Freeze-Drying Using Hydroxypropyl-beta-Cyclodextrin as Excipient. *Pharmaceutics* 13 (5). <https://doi.org/10.3390/pharmaceutics13050615>.
- Longest, P.W., Golshahi, L., Behara, S.R., Tian, G., Farkas, D.R., Hindle, M., 2015. Efficient Nose-to-Lung (N2L) Aerosol Delivery with a Dry Powder Inhaler. *J Aerosol Med Pulm Drug Deliv* 28 (3), 189–201. <https://doi.org/10.1089/jamp.2014.1158>.
- Marigo, M., Cairns, D.L., Davies, M., Ingram, A., Stitt, E.H., 2011. Developing mechanistic understanding of granular behaviour in complex moving geometry using the Discrete Element Method Part B: Investigation of flow and mixing in the Turbula (R) mixer. *Powder Technol* 212 (1), 17–24. <https://doi.org/10.1016/j.powtec.2011.04.009>.
- McGregor, D., 2010. Tertiary-Butanol: a toxicological review. *Crit Rev Toxicol* 40 (8), 697–727. <https://doi.org/10.3109/1040844.2010.494249>.
- Meinhardt, J., Radke, J., Dittmayer, C., Franz, J., Thomas, C., Mothes, R., Laue, M., Schneider, J., Brunink, S., Greuel, S., Lehmann, M., Hassan, O., Aschman, T., Schumann, E., Chua, R.L., Conrad, C., Eils, R., Stenzel, W., Windgassen, M., Rossler, L., Goebel, H.H., Gelderblom, H.R., Martin, H., Nitsche, A., Schulz-Schaeffer, W.J., Hakroush, S., Winkler, M.S., Tampe, B., Scheibe, F., Kortvellyessy, P., Reinhold, D., Siegmund, B., Kuhl, A.A., Elez Kurtaj, S., Horst, D., Oesterhelweg, L., Tsokos, M., Ingold-Heppner, B., Stadelmann, C., Drosten, C., Corman, V.M., Radbruch, H., Heppner, F.L., 2021. Olfactory transmucosal SARS-CoV-2 invasion as a part of central nervous system entry in individuals with COVID-19. *Nat Neurosci* 24 (2), 168–175. <https://doi.org/10.1038/s41593-020-00758-5>.
- Miwako, I., Kagechika, H., 2007. Tamibarotene. *Drugs Today* 43 (8), 563–568. <https://doi.org/10.1358/dot.2007.43.8.1072615>.
- Nizić Nodilo, L., Ugrina, I., Špoljarić, D., Amidžić Klarić, D., Jakobišić Brala, C., Perkušić, M., Pepić, I., Lovrić, J., Saršon, V., Safundžić Kućuk, M., Zadravec, D., Kalogjera, L., Hafner, A., 2021. A Dry Powder Platform for Nose-to-Brain Delivery of Dexamethasone: Formulation Development and Nasal Deposition Studies. *Pharmaceutics* 13 (6), 795. <https://doi.org/10.3390/pharmaceutics13060795>.
- Okuda, T., Tang, P., Yu, J., Finlay, W.H., Chan, H.K., 2017. Powder aerosol delivery through nasal high-flow system: In vitro feasibility and influence of process conditions. *Int J Pharm* 533 (1), 187–197. <https://doi.org/10.1016/j.ijpharm.2017.08.079>.
- Piepenbrink, M.S., Park, J.-G., Oladunni, F.S., Deshpande, A., Basu, M., Sarkar, S., Loos, A., Woo, J., Lovolenti, P., Sloan, D., Ye, C., Chiem, K., Bates, C.W., Burch, R.E., Erdmann, N.B., Goepfert, P.A., Truong, V.L., Walter, M.R., Martinez-Sobrido, L., Kobie, J.J., 2021. Therapeutic activity of an inhaled potent SARS-CoV-2 neutralizing human monoclonal antibody in hamsters. *Cell Rep Med* 2 (3), 100218. <https://doi.org/10.1016/j.xcrm.2021.100218>.
- Platto, S., Xue, T., Carafoli, E., 2020. COVID19: an announced pandemic. *Cell Death Dis* 11 (9), 799. <https://doi.org/10.1038/s41419-020-02995-9>.
- Porion, P., Sommier, N., Evesque, P., 2000. Dynamics of mixing and segregation processes of grains in 3d blender by NMR imaging investigation. *Europhys Lett* 50 (3), 319–325. <https://doi.org/10.1209/epl/i2000-00273-1>.
- Salian, V.S., Wright, J.A., Vedell, P.T., Nair, S., Li, C., Kandimalla, M., Tang, X., Carmona Porquera, E.M., Kalari, K.R., Kandimalla, K.K., 2021. COVID-19 Transmission, Current Treatment, and Future Therapeutic Strategies. *Mol Pharm* 18 (3), 754–771. <https://doi.org/10.1021/acs.molpharmaceut.0c0060810.1021/acs.molpharmaceut.0c00608.s00110.1021/acs.molpharmaceut.0c00608.s002>.
- Shang, J., Ye, G., Shi, K., Wan, Y., Luo, C., Aihara, H., Geng, Q., Auerbach, A., Li, F., 2020. Structural basis of receptor recognition by SARS-CoV-2. *Nature* 581 (7807), 221–224. <https://doi.org/10.1038/s41586-020-2179-y>.

- Sommier, N., Porion, P., Evesque, P., Leclerc, B., Tchoreloff, P., Couarraze, G., 2001. Magnetic resonance imaging investigation of the mixing-segregation process in a pharmaceutical blender. *Int J Pharm* 222 (2), 243–258. [https://doi.org/10.1016/S0378-5173\(01\)00718-9](https://doi.org/10.1016/S0378-5173(01)00718-9).
- Stella, V.J., Rao, V.M., Zannou, E.A., Zia, V.V., 1999. Mechanisms of drug release from cyclodextrin complexes. *Adv Drug Deliv Rev* 36 (1), 3–16. [https://doi.org/10.1016/S0169-409X\(98\)00052-0](https://doi.org/10.1016/S0169-409X(98)00052-0).
- Sungnak, W., Huang, N., Becavin, C., Berg, M., Queen, R., Litvinukova, M., Talavera-Lopez, C., Maatz, H., Reichart, D., Sampaziotis, F., Worlock, K.B., Yoshida, M., Barnes, J.L., Biological, H.L., 2020. SARS-CoV-2 entry factors are highly expressed in nasal epithelial cells together with innate immune genes. *Nat Med* 26 (5), 681–687. <https://doi.org/10.1038/s41591-020-0868-6>.
- Takeda, Y., Uchiyama, H., Matsuda, S., Ogawa, H., 2020. Acidic electrolyzed water potentially inactivates SARS-CoV-2 depending on the amount of free available chlorine contacting with the virus. *Biochem Biophys Res Commun* 530 (1), 1–3. <https://doi.org/10.1016/j.bbrc.2020.07.029>.
- Tiozzo Fasiolo, L., Manniello, M.D., Tratta, E., Buttini, F., Rossi, A., Sonvico, F., Bortolotti, F., Russo, P., Colombo, G., 2018. Opportunity and challenges of nasal powders: Drug formulation and delivery. *Eur J Pharm Sci* 113, 2–17. <https://doi.org/10.1016/j.ejps.2017.09.027>.
- Trenkel, M., Scherliess, R., 2021. Nasal Powder Formulations: In-Vitro Characterisation of the Impact of Powders on Nasal Residence Time and Sensory Effects. *Pharmaceutics* 13 (3), 385. <https://doi.org/10.3390/pharmaceutics13030385>.
- Wang, W., Xu, Y., Gao, R., Lu, R., Han, K., Wu, G., Tan, W., 2020. Detection of SARS-CoV-2 in Different Types of Clinical Specimens. *JAMA* 323 (18), 1843–1844. <https://doi.org/10.1001/jama.2020.3786>.
- Winchester, S., John, S., Jabbar, K., John, I., 2021. Clinical efficacy of nitric oxide nasal spray (NONS) for the treatment of mild COVID-19 infection. *J Infect* 83 (2), 237–279. <https://doi.org/10.1016/j.jinf.2021.05.009>.
- Wu, Z., Harrich, D., Li, Z., Hu, D., Li, D., 2021. The unique features of SARS-CoV-2 transmission: Comparison with SARS-CoV, MERS-CoV and 2009 H1N1 pandemic influenza virus. *Rev Med Virol* 31 (2), e2171. <https://doi.org/10.1002/rmv.2171>.
- Yuan, S.F., Chan, C.C.Y., Chik, K.K.H., Tsang, J.O.L., Liang, R.H., Cao, J.L., Tang, K.M., Cai, J.P., Ye, Z.W., Yin, F.F., To, K.K.W., Chu, H., Jin, D.Y., Hung, I.F.N., Yuen, K.Y., Chan, J.F.W., 2020. Broad-Spectrum Host-Based Antivirals Targeting the Interferon and Lipogenesis Pathways as Potential Treatment Options for the Pandemic Coronavirus Disease 2019 (COVID-19). *Viruses* 12 (6), 628. <https://doi.org/10.3390/v12060628>.
- Yuan, S.F., Chu, H., Chan, J.F.W., Ye, Z.W., Wen, L., Yan, B.P., Lai, P.M., Tee, K.M., Huang, J.J., Chen, D.D., Li, C., Zhao, X.Y., Yang, D., Chiu, M.C., Yip, C., Poon, V.K.M., Chan, C.C.S., Sze, K.H., Zhou, J., Chan, I.H.Y., Kok, K.H., To, K.K.W., Kao, R.Y.T., Lau, J.Y.N., Jin, D.Y., Perlman, S., Yuen, K.Y., 2019. SREBP-dependent lipidomic reprogramming as a broad-spectrum antiviral target. *Nat Commun* 10 (1), 120. <https://doi.org/10.1038/s41467-018-08015-x>.
- Zhao, J., Zhao, S., Ou, J., Zhang, J., Lan, W., Guan, W., Wu, X., Yan, Y., Zhao, W., Wu, J., Chodosh, J., Zhang, Q., 2020. COVID-19: Coronavirus Vaccine Development Updates. *Front Immunol* 11, 602256. <https://doi.org/10.3389/fimmu.2020.602256>.
- Ziegler, C.G.K., Allon, S.J., Nyquist, S.K., Mbano, I.M., Miao, V.N., Tzouanas, C.N., Cao, Y., Yousif, A.S., Bals, J., Hauser, B.M., Feldman, J., Muus, C., Wadsworth, M.H., Kazer, S.W., Hughes, T.K., Doran, B., Gatter, G.J., Vukovic, M., Taliaferro, F., Mead, B.E., Guo, Z., Wang, J.P., Gras, D., Plaisant, M., Ansari, M., Angelidis, I., Adler, H., Sucre, J.M.S., Taylor, C.J., Lin, B., Waghay, A., Mitsialis, V., Dwyer, D.F., Buchheit, K.M., Boyce, J.A., Barrett, N.A., Laidlaw, T.M., Carroll, S.L., Colonna, L., Tkachev, V., Peterson, C.W., Yu, A., Zheng, H.B., Gideon, H.P., Winchell, C.G., Lin, P. L., Bingle, C.D., Snapper, S.B., Kropski, J.A., Theis, F.J., Schiller, H.B., Zaragosi, L.-E., Barbry, P., Leslie, A., Kiem, H.-P., Flynn, J.L., Fortune, S.M., Berger, B., Finberg, R.W., Kean, L.S., Garber, M., Schmidt, A.G., Lingwood, D., Shalek, A.K., Ordovas-Montanes, J., Banovich, N., Barbry, P., Brazma, A., Desai, T., Duong, T.E., Eickelberg, O., Falk, C., Farzan, M., Glass, I., Haniffa, M., Horvath, P., Hung, D., Kaminski, N., Krasnow, M., Kropski, J.A., Kuhnemund, M., Lafyatis, R., Lee, H., Leroy, S., Linnarson, S., Lundeberg, J., Meyer, K., Misharin, A., Nawijn, M., Nikolic, M.Z., Ordovas-Montanes, J., Pe'er, D., Powell, J., Quake, S., Rajagopal, J., Tata, P.R., Rawlins, E.L., Regev, A., Reyfman, P.A., Rojas, M., Rosen, O., Saeb-Parsy, K., Samakovlis, C., Schiller, H., Schultze, J.L., Seibold, M.A., Shalek, A.K., Shepherd, D., Spence, J., Spira, A., Sun, X., Teichmann, S., Theis, F., Tskov, A., van den Berge, M., von Papen, M., Whitsett, J., Xavier, R., Xu, Y., Zaragosi, L.-E., Zhang, K., 2020. SARS-CoV-2 Receptor ACE2 Is an Interferon-Stimulated Gene in Human Airway Epithelial Cells and Is Detected in Specific Cell Subsets across Tissues. *Cell* 181 (5), 1016–1035.e19. <https://doi.org/10.1016/j.cell.2020.04.035>.